1995

Synthesis, Characterization, and Molecular Structure of Bis(tetraphenylcyclopentdienyl)rhodium(II)⊗

James E. Collins

Michael Castellani
Marshall University, castella@marshall.edu

Arnold L. Rheingold

Edward J. Miller

William E. Geiger

See next page for additional authors

Authors

James E. Collins, Michael Castellani, Arnold L. Rheingold, Edward J. Miller, William E. Geiger, Anne L. Rieger, and Philip H. Rieger

Synthesis, Characterization, and Molecular Structure of

Bis(tetraphenylcyclopentdienyl)rhodium(II)$^{\otimes}$

James E. Collins,[†] Michael P. Castellani,[*,†] Arnold L. Rheingold,[*,‡] Edward J. Miller,[§,♦]

William E. Geiger,[*,§] Anne L. Rieger,[∇] and Philip H. Rieger[*,∇]

Departments of Chemistry, Marshall University, Huntington, West Virginia 25755;

University of Delaware, Newark, Delaware, 19716; University of Vermont, Burlington,

Vermont, 05405; and Brown University, Providence, Rhode Island, 02912.

Abstract

A 5 day diglyme reflux of $Rh(acac)_3$ and $K(C_5HPh_4)$, followed by treatment with aqueous HPF_6, produces orange-yellow $[(C_5HPh_4)_2Rh]PF_6$ in 40 - 50% yield. Reduction of $[(C_5HPh_4)_2Rh]PF_6$ with sodium amalgam in THF yields olive green $(C_5HPh_4)_2Rh$ in 70% yield. $(C_5HPh_4)_2Rh$ crystallizes in the triclinic $P\bar{1}$ space group with unit-cell parameters of $a = 8.622$ (3) Å, $b = 10.778$ (4) Å, $c = 12.894$ (5) Å, $\alpha = 65.58$ (3)°, $\beta = 72.66$ (3)°, $\gamma = 83.52$ (3)°, and $Z = 1$. The least squares data refined to $R_F = 7.63\%$ and $R_{wF} = 10.12\%$ for the 2479 independent observed reflections with $F_o > 5\sigma(F_o$). The metal-centroid distance is 1.904 Å and all other bond lengths and angles are similar to known octaphenylmetallocenes. ESR spectra of $(C_5HPh_4)_2Rh$ in low-temperature glasses display a rhombic *g*-tensor with resolution of Rh hyperfine splitting on one-*g*-component. Analysis of the spectral parameters is consistent with a d^7 configuration derived from a nearly degenerate d_{xz}, d_{yz} ground state. Voltammetry and coulometry establish the electron-transfer series $(C_5HPh_4)_2Rh^{1+/0/1-}$ with $E°$ values of -1.44 V and -2.13 V *vs* ferrocene. The heterogeneous charge transfer rate of the second reduction is about three orders of magnitude lower than that of the first.

1

†Marshall University

‡University of Delaware

§University of Vermont

$^\nabla$Brown University

$^\otimes$Dedicated to Prof. Harry E. Persinger on the occasion of his seventy-fifth birthday.

♦Permanent address: State University of New York, College at Plattsburgh, Plattsburgh, N.Y. 12901

Introduction

Neutral metallocenes of most of the first-row transition metals exist as thermally stable, crystalline solids. Although many of these compounds are paramagnetic, far fewer examples of open shell metallocenes are known for the lower rows. Low temperature studies have provided some such examples.[1, 2] In 1985 Cloke and co-workers prepared decamethylrhenocene, (η^5-$C_5Me_5)_2Re$,[3] which represents the only isolable, open shell, lower row neutral metallocene proven to exist.[4] Decaphenylmolybdocene[5] and (η^5-$C_5Me(CO_2Me)_4)_2Rh$[6] have been reported; however, definitive proof of their identities was not provided. In this paper we report the synthesis and characterization of octaphenylrhodocene and its oxidation product.

In 1953, Wilkinson and co-workers[7] reported the synthesis of the rhodicinum cation, Cp_2Rh^+, from the reaction of $Rh(acac)_3$ and CpMgBr (acac = 2,4-pentanedionate, Cp = η^5-C_5H_5). Keller and Wawersik trapped Cp_2Rh on a liquid nitrogen cooled ESR probe after a reductive sublimation of Cp_2Rh^+ by molten sodium.[8] Warming above 77 K resulted in the complex dimerizing through one ligand on each of two rhodocene molecules to yield a closed shell product (eq 1).[9] Thus, spectroscopic characterization of rhodocene is largely limited to its

$$2\ [(C_5H_5)_2Rh]PF_6\ +\ Na(l)\ \xrightarrow{77\ K}\ 2\ \left[\begin{array}{c} Rh \end{array} \right] \xrightarrow{\Delta} \qquad (1)$$
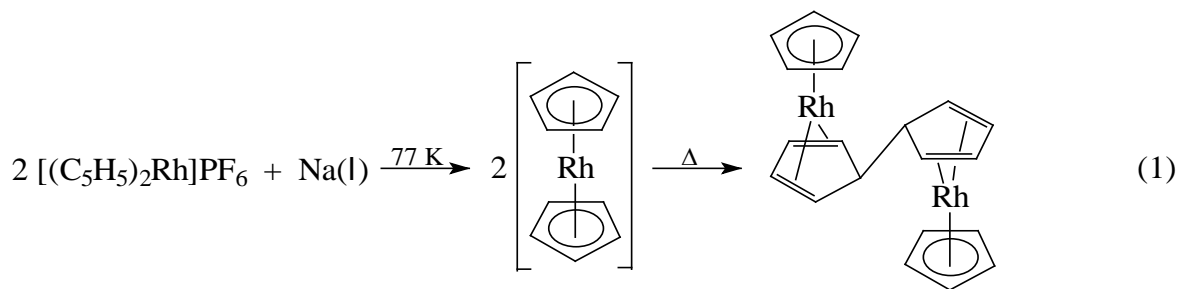
ESR spectrum. The transient existence of rhodocene at ambient temperature has also been observed in electrochemical[10] and mass spectral[11] studies of Cp_2Rh^+.

Polyphenylated cyclopentadienyl ligands frequently reduce the reactivity of complexes in which they are incorporated.[12] The very large size of the tetraphenylcyclopentadienyl ligand (η^5-C_5HPh_4) suggested that the dimerization reaction that occurred for Cp_2Rh would not happen for $(C_5HPh_4)_2Rh$. The phenyl substituents should also prevent close approach of substrates that might displace a cyclopentadienyl ligand. Finally, an internal reaction (e.g. orthometallation)

3

would probably generate a complex with an unstable metal oxidation state, electron count, or ligand geometry.

Experimental Section

General Data. All reactions of air- and moisture-sensitive materials were performed under an argon atmosphere employing standard Schlenk techniques, unless otherwise noted. Solids were manipulated under argon in a Vacuum Atmospheres glovebox equipped with an HE-493 dri-train. Hydrated rhodium(III) chloride, hydrated iridium(III) chloride (Johnson-Mathey), 2,4-pentanedione (Aldrich), and 60% aqueous HPF_6 (Strem) were used as received. $K(C_5HPh_4)\cdot0.5THF$[13] and $Tl(C_5HPh_4)$[14] were prepared according to literature procedures. Solvents were distilled from an appropriate drying agent under argon: diglyme, triglyme (Aldrich), toluene and hexane (Fisher) (sodium/benzophenone ketyl), benzene and tetrahydrofuran (THF) (Fisher) (potassium/benzophenone ketyl), and dichloromethane (Fisher) (CaH_2). All other solvents were used as received. Elemental analyses were performed by Schwarzkopf Microanalytical Laboratory, Woodside, NY.

^{1}H NMR spectra (200.06 MHz) were obtained on a Varian XL-200 NMR spectrometer equipped with a Motorola data system upgrade. Melting points are uncorrected.

Electrochemistry. Voltametric and coulometric experiments were conducted as previously described.[15] Potentials are referred to the ferrocene (Fc)/ferrocenium couple. The supporting electrolyte was $[Bu_4N][PF_6]$ in all cases. Voltammetry simulations employed the method of Grosser.[16]

ESR Spectroscopy.   X-band ESR spectra were obtained using a Bruker ESP300E spectrometer at the University of Bristol. The spectrometer was equipped with a liquid nitrogen Dewar flask and a variable temperature unit; field-frequency calibration relied on a Hewlett-Packard microwave frequency counter and the Bruker Hall probe, the offset of which was checked from time to time with DPPH. Toluene solutions of $(C_5HPh_4)_2Rh$ were prepared for ESR spectral studies in several ways, including the use of a nitrogen-filled glovebox, modified

Schlenk techniques, and a vacuum line.

Tris(acetylacetonato)rhodium(III), 1. Tris(acetylacetonato)rhodium(III) was prepared by modifying a literature procedure.[17] All steps were carried out in the air. Hydrated rhodium(III) chloride (2.50 g, 9.50 mmol) was dissolved in distilled H_2O (20 mL). The pH of the solution was adjusted to the range 4.00-5.00 by dropwise addition of aqueous 10% $NaHCO_3$. When necessary, 0.1 M HCl was used as a back titrating reagent. The deep purple solution was then treated with 2,4-pentanedione (9.0 mL, 87 mmol), and refluxed for 30 min. After allowing the solution to cool to room temperature, the pH of the system was re-adjusted to the range 4.00-5.00. Precipitation of $Rh(acac)_3$ occurred during this process. This mixture (without filtering) was refluxed for 24 h during which time the color of the reaction solution lightened considerably. The orange-yellow solid was collected by vacuum filtration and recrystallized from boiling methanol. The hot methanol solution was slowly cooled, followed by further cooling in an ice-water bath to produce orange-yellow, crystalline **1** (2.78 g, 73%). Mp: 260-263 °C (lit. 260 °C).

Tris(acetylacetonato)iridium(III). This synthesis was the same as for **1** except that $IrCl_3 \cdot nH_2O$ was used in place of $RhCl_3 \cdot nH_2O$ in the same molar amount. Yield: 45%.

Bis(tetraphenylcyclopentadienyl)rhodium(III) Hexafluorophosphate, 2. Diglyme (15 mL) was added to a solid mixture of $Rh(acac)_3$ (0.25 g, 0.62 mmol) and $K(C_5HPh_4) \cdot 0.5THF$ (0.55 g, 1.2 mmol). The reaction mixture was refluxed for 5 d. The dark green/brown solution was transferred to a plastic cup in the air while cooling to room temperature and the green color immediately disappeared. Aqueous HPF_6 (1 mL) was added to the stirring solution. After one hour, the solution was filtered and the resulting yellow powder was washed with diethyl ether followed by water. The yellow solid was oven dried at 100 °C for 24 h and then extracted with CH_2Cl_2. The resulting solution was gravity filtered into a test tube and layered with an equal volume of hexane. Slow diffusion of the layers yielded large, straw-like yellow crystals of **2** (0.28 g, 46 %). Mp: 409 °C (dec). ^{1}H NMR (CD_2Cl_2) δ 6.8-7.5 (m). Anal. Calcd for $C_{58}H_{42}F_6PRh$: C, 70.59; H, 4.29. Found: C, 70.95; H, 4.52.

Bis(tetraphenylcyclopentadienyl)rhodium(II), 3. A THF slurry (25 mL) of **2** (0.20 g,

0.20 mmol) was degassed by the freeze-pump-thaw method. This mixture was transferred via cannula onto a 0.1% sodium amalgam (9.3 mg, 0.41 mmol Na). The reaction mixture was stirred vigorously until there was no evidence of the yellow rhodocenium salt suspension (*ca.* 45 min). The olive green solution was transferred to another flask via cannula to prevent further reduction[18] and the THF was removed *in vacuo*. The solid was extracted into boiling toluene, frit filtered, and the resulting solution was concentrated to near saturation. Hexane (10 mL) was added and the resulting solution was cooled to -20 °C overnight to yield deep olive-green microcrystals of **3** (0.12 g, 70%). Recrystallization of **3** was performed by slow diffusion of hexane into a saturated benzene solution of **3**. Mp: 311-313 °C. Anal. Calcd for $C_{58}H_{42}Rh$: C, 82.75; H, 5.03. Found: C, 82.74; H, 4.84. Visible λ_{max} (THF): 715 nm (5.79 x 10^3 $M^{-1}cm^{-1}$).

X-Ray Diffraction Study of Bis(tetraphenylcyclopentadienyl)rhodium(II). A crystal of $(C_5HPh_4)_2Rh$ was grown by layer diffusion of hexane into a saturated THF solution of **3**. Crystal data and parameters used during the collection of intensity data are given in Table I. A dark green crystal was mounted on a fine glass fiber with epoxy cement. It crystallized in the triclinic space group $P\bar{1}$ and is isomorphous with the other, previously reported octaphenylmetallocenes.[13, 19, 20] Unit-cell dimensions were derived from a least-squares fit of the angular settings of 25 reflections with 20° < 2θ < 25°. A profile fitting procedure was applied to all intensity data to improve the precision of the measurement of weak reflections. Reflections were corrected for absorption effects using the program XABS (H. Hope), which is based on deviations in F_o and F_c values.

The structure was solved by taking the coordinates of the previously determined octaphenylferrocene, replacing Rh for Fe, and allowing the structure to refine. All hydrogen atoms were treated as idealized, isotropic contributions (d(C-H) = 0.96 Å, U = 1.2 U_{iso} of attached C). Atomic positions, bond distances, and bond angles are collected in Tables II-III, respectively. All computer programs used in the data collections and refinements are contained in the Siemens programs P3 and SHELXTL PLUS (VMS).

Results and Discussion

Synthesis and Reactivity. A five day reflux of $Rh(acac)_3$ and $K(C_5HPh_4)$ in diglyme, after treatment with aqueous HPF_6, produces $[(C_5HPh_4)_2Rh]PF_6$, **2**, in 40 - 50% yield as an orange-yellow, crystalline solid (eq 2). The $Rh(acac)_3$ was prepared by a modified literature

$$Rh(acac)_3 + 2\ K(C_5HPh_4) \xrightarrow[\text{2) HPF}_6\text{(aq)}]{\text{1) diglyme, }\Delta} [(C_5HPh_4)_2Rh]PF_6 + 2\ KPF_6 + 3\ Hacac \quad (2$$

procedure (*vida supra*).[17] Substantial yield reductions occur with shorter reaction times and reactions employing lower boiling THF as solvent produce none of the desired product. $[(C_5HPh_4)_2Rh]PF_6$ is soluble in CH_2Cl_2, slightly soluble in THF and acetone, and poorly soluble or insoluble in most other solvents. It is air-stable.

Attempts to prepare the analagous octaphenyliridicinium complex, $(C_5HPh_4)_2Ir^+$, using a variety of reagents and conditions were unsuccessful (eq 3 - 4, M = K or Tl). Refluxes were

$$Ir(acac)_3 + 2\ M(C_5HPh_4) \xrightarrow[\text{triglyme, }\Delta]{\text{diglyme or}} No\ Reaction \quad (3$$

$$IrCl_3 \cdot 2 H_2O + 2\ M(C_5HPh_4) \xrightarrow[\text{triglyme, }\Delta]{\text{diglyme or}} No\ Reaction \quad (4$$

carried out for up to 7 days with periodic checks made for the generation of $(C_5HPh_4)_2Ir^+$. The behavior observed in this system is reminiscent of that which occurs for the metals of the iron group.[21]

Reduction of $[(C_5HPh_4)_2Rh]PF_6$ by 0.1% sodium amalgam in THF produces olive green $(C_5HPh_4)_2Rh$, **3**, in 70% yield (eq 5). Octaphenylrhodocene is the most air-sensitive of the

$$[(C_5HPh_4)_2Rh]PF_6 + Na/Hg \xrightarrow{\text{THF}} (C_5HPh_4)_2Rh + NaPF_6 \quad (5)$$

octaphenylmetallocenes reported to date; decomposing instantly in solution and in minutes as a solid upon exposure to the air. Thus **3** is dramatically more oxygen-sensitive than its congener $(C_5HPh_4)_2Co$, but is similar to $(C_5HPh_4)_2V$.[13] This is probably because of the greater accessibility of the metal in **3** and the lower stability of Rh(II) as compared to Co(II). Compound **3** reacts slowly with CH_2Cl_2, although it does so more rapidly than $(C_5HPh_4)_2Co$. This behavior

is also consistent with the phenyl rings preventing close approach of even small substrates to the rhodium center. Complex **3** is quite thermally stable; however, and melts sharply at 311 °C. It is soluble in benzene, toluene, and THF.

Molecular Structure. The crystal structure of $(C_5HPh_4)_2Rh$ is isomorphous to the other known octaphenylmetallocenes.[13, 19, 20] It crystallizes as discrete, well-separated molecules with a staggered C_5 configuration and a Rh atom on a crystallographic center of symmetry (Figure 1). Bond distances and angles are collected in Table III. The M-CNT distance increases from 1.771 Å in $(C_5HPh_4)_2Co$ to 1.904 Å in $(C_5HPh_4)_2Rh$ which is close to the corresponding increase in metal covalent radius (0.09 Å).[22] The average Rh-C distances in **3** (2.26 Å) also increase in comparison to $(C_5HPh_4)_2Ru$ (2.20 Å)[20] and $(C_5H_3(CO_2Me)_3)_2Rh^+$ (2.17 Å).[23] This is consistent with the 19th electron residing in an anti-bonding orbital. The phenyl torsion angles (Table IV) are similar to those of $(C_5HPh_4)_2Ru$.

Electrochemistry. Solutions of substituted rhodocenium cation **2** gave two well-defined voltammetric waves (Figure 2) in nonaqueous solvents such as CH_3CN, DMF, and THF. As shown below, they are consistent with the step-wise formation of the neutral complex, **3**, and the nominally 20e anion $(C_5HPh_4)_2Rh^-$, **4**. Although the anion is much longer lived than its unsubstituted analogue (the lifetime of Cp_2Rh^- is *ca.* 0.02 s at room temperature[10a]), it splits off $C_5HPh_4^-$ on the bulk electrolysis time scale. It will also be shown that the heterogeneous electron transfer rate for reduction of **3** to **4** is much slower than that of the oxidation of **3** to **2**.

Reduction of 2 to 3. The first reduction of **2** is essentially Nernstian at both Pt and Hg electrodes, with $E°_{2/3}$ = -1.44 V *vs* Fc. Over the scan rate range of v = 0.05 to 0.50 V/s, values of ΔE_p ($= E_{pa} - E_{pc}$) and δE_p ($= E_{pc/2} - E_{pc}$) of 63 ± 5 mV and 64 mV were measured, respectively, close to the values expected for electrochemically reversible couples.[24] The k_s value for the couple appears to be > 1 cm/s.

Bulk coulometry confirmed the one-electron nature of this reduction. Electrolysis (E_{appl} = -1.7 V) in THF at ambient temperatures of *ca.* 0.5mM solutions of **2** in DMF or THF consumed 1.0 F per mole and resulted in green solutions of **3** that were stable for weeks if kept under N_2.

Voltammetry of the electrolysis solution at the rotating Pt electrode (RPE) showed that conversion from **2** to **3** was quantitative (Figure 3).

The second reduction of **2** involves irreversibility, in both the electrochemical and chemical senses. The stoichiometry of the second reduction is best established by high overpotential methods such as RPE voltammetry and chronoamperometry. Figure 2 (top) shows that the reduction with $E_{1/2}$ *ca.*-2.2 V is a one-electron process, with a relative plateau current equal to that of the **2/3** couple. The same 1e stoichiometry is implied by chronoamperometry results on solutions of **2**, which show that stepping beyond the second wave gives an it$^{1/2}$ constant (42.0 $\mu A\ s^{-1/2}$) about double that of the first wave (19.6 $\mu A\ s^{-1/2}$) for a 5 s pulse.

The one-electron product **4** implied by these results is not stable over the time scale of a bulk electrolysis (*ca.* 20 min). Electrolysis potentials past the second wave (E_{appl} = -2.6 V) required 2-3e beyond that required to form **3** and resulted in a partially reversible product wave with E_{pa} = -0.74 V, exactly the potential measured for a sample of $K(C_5HPh_4)$. Thus it appears that **4** eventually releases at least one of its ligands. The overall electron transfer series involving this rhodocenium analogue can therefore be written as:

$$(C_5HPh_4)_2Rh^+ + e^- \rightleftharpoons (C_5HPh_4)_2Rh \tag{6}$$

$$(C_5HPh_4)_2Rh + e^- \rightleftharpoons (C_5HPh_4)2Rh^- \tag{7}$$

$$(C_5HPh_4)_2Rh^- \rightarrow C_5HPh_4^- + (C_5HPh_4)Rh\ (solv) \tag{8}$$
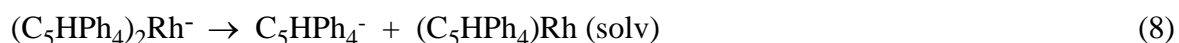
It is likely that a solvated complex (eq 8) is formed when $C_5HPh_4^-$ splits off, although the counter ion mght also coordinate to the metal fragment, especially in CH_2Cl_2. The half-sandwich fragment is also electroactive at the E_{appl} of the electrolysis and undergoes reduction by at least one more electron, resulting in higher coulometric counts and most likely the release of the second tetraphenylcyclopentadienyl ligand from the metal.

The anion **4** appears to be stable, however, at room temperature, on the cyclic voltammetry (CV) and chronoamperometry (5 s) time scales. As the following discussion will show, the couple **3** + e$^-$ $\rightleftharpoons$ **4** is complicated by slow charge transfer kinetics, so that its CV waves may be analyzed as an (electrochemically) irreversible system.

CV scans of **2** yield the following qualitative observations concerning the behavior of the second wave: (1) it has a lower cathodic peak height than the first (*ca.* 0.8 for i_{p2}/i_{p1}), (2) its (anodic) reverse response is broader than that of the cathodic wave, and (3) the ΔE_p value is greatly increased over the Nernstian value. Further experiments show that the positions of both the cathodic wave and coupled anodic wave are highly dependent on sweep rate, moving to more negative and positive values, respectively, with higher *v*. Each of these observations is consistent with a couple that is *chemically reversible* (stable **3** and **4** on the experimental time scale) but *electrochemically irreversible* (slow heterogeneous electron transfer kinetics for **3** + e⁻ $\rightleftharpoons$ **4**). It should also be noted that the peak separations for this couple, while qualitatively similar, were somewhat electrode (Hg, Au, Pt) and solvent dependent. A typical set of data taken in DMF at Pt and Hg electrodes is discussed below.

Slow charge-transfer (quasi- or ir-reversible) systems are characterized by the parameters $E°$, α (transfer coefficient), and k_s (heterogeneous electron transfer rate at $E°$).[25] Three methods employed for measurement of α gave consistent results with α = *ca.* 0.6. The breadth of the wave, given by $\delta E_p = E_{p/2} - E_p$ gives α from the relationship δE_p = 48 mV/αn.[26] Over the scan rate range of 0.05 to 0.50 V/s, the experimental average of 80 mV for δE_p suggests an α value of 0.60. This value of α predicts a negative shift for E_p of 50 mV (= 48 mV/αn)[26] per tenfold increase in *v*, approximately what is observed for the couple at a Hg electrode.[27] Lastly, the cathodic peak height for an irreversible system with α = 0.6 should be about 85% of that of a reversible system with the same diffusion coefficient,[28] consistent with our observation that the ratio of the second cathodic peak current (extrapolated from the continuation of the first wave) is about 0.80 times the value of the first cathodic peak current.

Some attempts were made at digital simulation of the two waves assuming the stepwise EE mechanism for the reduction of **2,** with the second reduction being much slower than the first. Moderate success was observed matching experiments at slower scan rates, but the data at higher sweep rates (above *ca.* 2 V/s) could not be fit with the same theoretical parameters, perhaps because of the very unusual shape of the anodic portion of the reverse wave. Figure 2 (bottom)

shows a typical low scan rate fit. The best fits at a Pt electrode were obtained with $E° = -2.13$ V

vs Fc, $k_s = ca.$ 10^{-3} cm/s, $\alpha = 0.63$ to 0.68.

We cannot rule out the possibility that the second reduction should be treated as an EC mechanism, in which a slow charge transfer is followed by a very fast structural rearrangement. The voltammetry seems to be suggesting that the anion **4** undergoes a significant structural rearrangement compared to **3**, as might be expected for a nominally 20e species. Certainly, ring slippage from η^5 to η^4 or η^3 is a possibility.[29] If such a distortion occurs, the present data do not allow us to say how much of the structure change occurs during, as opposed to subsequent to, the electron transfer transition state.

It is of interest to compare the potentials measured for the system **2/3/4** with those reported for the reduction of other rhodocenium type complexes. These are collected in Table V. It is perhaps most relevant to compare the separation of the two $E°$ values for reduction of the 18/19e and 19/20e couples. The value of -690 mV measured for $E°_{3/4}$ - $E°_{2/3}$ for the present system is very close to that (-770 mV) measured by Holloway and co-workers, for the parent system, $Cp_2Rh^{+/0/-}$ at severely reduced temperatures.[10a] A similar separation (-700 mV) has been recently reported for reduction of the indenyl derivative $(\eta^5-C_5Me_5)Rh(\eta^5-C_9H_7)^+$ by Gusev and co-workers.[10b] On the other hand, the much larger separations reported for the reduction of $(C_5Me_5)Rh(C_5R_5)$ cations (R = H, Me)[16] suggest that the second reduction waves of the latter systems involve a structure other than the 19e radical intermediate, perhaps one with a dimeric structure.

Finally, it is worth noting that the substitution of two tetraphenylcyclopentadienyl units for cyclopentadienyl units shifts the $E°$ values of the Rh sandwich complexes 370 mV more positive, reflecting an appreciable thermodynamic stabilization of the lower oxidation state by the C_5HPh_4 ligand compared to C_5H_5. This value is larger than those (50-200 mV) reported for a number other octaphenylmetallocenes reported earlier.[13]

ESR Spectra. Spectra of $(C_5HPh_4)_2Rh$ in a toluene glass at 77 or 90 K show three features, characteristic of a rhombic g-tensor and quite different from the broad, apparently axial,

spectrum reported for Cp_2Rh.[8] Although the spectrum was generally reproducible, thawing and refreezing of a sample resulted in slightly different positions of the features. The measured g-tensor components for five spectra are given in Table VI. The low-field feature is a singlet at 90 K, but is resolved into a doublet at 77 K (a^{Rh} = 26 G, components widths *ca.* 20 G), but the central and high-field features remain unresolved with widths of *ca.* 40 and 70 G, respectively.

In a d^7 metallocene with D_{5h} symmetry, d_{xz} and d_{yz} belong to the $\mathbf{e_1}''$ representation and the ground state is degenerate, leading to dynamic Jahn-Teller distortions. In $(C_5HPh_4)_2Rh$, with at most C_i symmetry, the d_{xz}/d_{yz} degeneracy is lifted, at least in principle, and one of these orbitals is expected to be singly occupied with the other low-lying and empty. If the splitting of the d_{xz}- and d_{yz}-based MO's is big enough, we would expect $g_z \ll g_e$ and g_x, $g_y > g_e$.[30] Such reasoning gives a good account of the g-tensor components in other Rh(II) complexes,[31] but for $(C_5HPh_4)_2Rh$, one of the "perpendicular" components is found to be less than g_e. Thus d_{xz} and d_{yz} are apparently nearly degenerate such that vibronic mixing of these orbitals must be taken into account.

Ammeter has described a model to account for the ESR spectra of mellocenes with degenerate or near-degenerate ground states.[32] In the model for d^7 metallocenes, it is assumed that the SOMO is a vibronic admixture of the static MO's with d_{xz} and d_{yz} character

$$\left| SOMO \right\rangle = c'\left(c_\pi \left| d_{xz} \right\rangle - c_\pi' \left| \phi_{xz}^\perp \right\rangle \right) \chi_{xz} + is'\left(c_\pi \left| d_{yz} \right\rangle - c_\pi' \left| \phi_{yz}^\perp \right\rangle \right) \chi_{yz} \qquad (9)$$

where $\left| \phi_{xz}^\perp \right\rangle$ and $\left| \phi_{yz}^\perp \right\rangle$ are appropriate combinations of ligand orbitals and χ_{xz} and χ_{yz} are relevant vibrational functions. According to this model, the g-tensor components are given by[32]

$$g_z = g_e - 2kV \cos \alpha \qquad (10a)$$

$$g_\perp = \tfrac{1}{2}(g_x + g_y) = (g_e + 5x) \sin \alpha \qquad (10b)$$

$$g_y - g_x = 6x \, (1 + V \cos \alpha) \qquad (10c)$$

where $\tan \alpha$ described the degree of d_{xz}/d_{yz} mixing,

$$\tan \alpha = \frac{c'^2 - s'^2}{2c's'} \qquad (11)$$

V is the vibrational overlap integral,

$$V = \langle \chi_{xz} | \chi_{yz} \rangle \tag{12}$$

x is proportional to $\zeta/\overline{\Delta E}$ where ζ is the spin-orbital coupling parameter and $\overline{\Delta E}$ is an average one-electron excitation energy, and k is the orbital angular momentum reduction factor resulting from delocalization of spin into ligand orbitals,

$$k = 1 - c'^2_\pi \left(1 - \langle \phi^L_{xz} | l_z | \phi^L_{yz} \rangle \right) \tag{13}$$

Ammeter finds $k = 0.85$ for the first-row metallocenes. If we assume $k = 0.85 \pm 0.10$ for octaphenylrhodocene and that the g-tensor components are accurate to ± 0.001, we obtain the values of $\tan \alpha$ and kV listed in Table VI.

A plot of kV *vs.* $\tan \alpha$, after Ammeter,[32a] is shown in Figure 4. The plot includes data for Cp_2Co and $(RCp)_2Co$, R = Me, Et, Bu^t, in variety of host lattices, and Cp_2Ni^+ in nine cobalticinium salt lattices; good linear correlations of kV with $\tan \alpha$ are obtained. The variation in these parameters with host lattice was ascribed to lattice-dependent vibronic mixing. The points for $(C_5HPh_4)_2Rh$, plotted on the same graph, lie very close to the cobaltocene correlation line, suggesting: (i) that the electronic structure and degree of vibronic mixing are similar for octaphenylrhodocene and cobaltocene; and (ii) that toluene glasses contain a variety of solvation sites, the distribution of which depends on the thermal history of the sample, in which various vibrational modes are differentially enhanced or suppressed.

The g-tensor components for $(C_5HPh_4)_2Co$ and $[(C_5HPh_4)_2Ni]^+$ from Trogler and coworkers[13] are also given in Table VI, and values of $\tan \alpha$ and kV are listed for octaphenylcobaltocene. The point corresponding to these values, plotted in Figure 5, is seen to lie far from the correlation line, suggesting that the Ammeter model is a poor approximation for $(C_5HPh_4)_2Co$. The parameters for the Ni(III) derivative cannot be fitted to eqs (10); it appears that $\alpha \approx 90°$, implying a large static splitting and negligible vibronic mixing of the d_{xz}- and d_{yz}-based MO's. Indeed, the g-components for $[(C_5HPh_4)_2Ni]^+$ are consistent with the static model discussed above.

For $(C_5HPh_4)_2M$, M = Rh, Co, and Ni, the x-ray structures show that the M-C(1) distance is significantly shorter than the average of the other M-C distances (by 2.3, 3.6 and 4.4% for Rh, Co, and Ni, respectively). This distortion from five-fold symmetry lifts the d_{xz}/d_{yz} degeneracy. Since the Ni-C distances are expected to be shorter in the cation, the relative difference between Ni-C(1) and the other Ni-C distances is probably even greater. Apparently the d_{xz}/d_{yz} splitting in $[(C_5HPh_4)_2Ni]^+$ is big enough to essentially eliminate vibronic mixing. In the Co(II) complex, the static splitting is apparently significant, but not large enough to completely eliminate vibronic mixing, and in octaphenylrhodocene, the splitting is sufficiently small that the molecule behaves as if it had a degenerate ground state.

Summary. This work describes the synthesis and characterization of $[(C_5HPh_4)_2Rh]PF_6$ and $(C_5HPh_4)_2Rh$. The compound represents the first isolated rhodocene and only the second isolated lower row, open-shell neutral metallocene. Aside from a high sensitivity to oxidation, it appears to be relatively non-reactive. ESR spectra of $(C_5HPh_4)_2Rh$ in low-temperature glasses display a rhombic g-tensor with resolution of Rh hyperfine splitting on one-*g*-component. Analysis of the spectral parameters is consistent with a d^7 configuration derived from a nearly degenerate d_{xz}, d_{yz} ground state. Voltammetry and coulometry establish the electron-transfer series $(C_5HPh_4)_2Rh^{1+/0/1-}$ with $E°$ values of -1.44 V and -2.19 V *vs* Fc. The heterogeneous charge transfer rate of the second reduction is much lower than that of the first.

Matthey made generous loans of $RhCl_3 \cdot nH_2O$ and $IrCl_3 \cdot nH_2O$.

Supplementary Material Available. For $(C_5HPh_4)_2Rh$ as follows: Table 1S, anisotropic displacement coefficients, and Table 2S, hydrogen-atom coordinates (2 pages). Ordering information is given on any current masthead page.

References

1. (a) Mo, W, Re: Graham, R. G.; Grinter, R.; Perutz, R. N. *J. Am. Chem. Soc.* **1988**, *110*, 7036. (b) Mo, W: Chetwynd-Talbot, J.; Grebenik, P.; Perutz, R. N. *Inorg. Chem.* **1982**, *21*, 3647. (c) Re: Chetwynd-Talbot, J.; Grebenik, P.; Perutz, R. N.; Powell, M. H. A. *Inorg. Chem.* **1983**, *22*, 1675.

2. Nb: (a) Elson, I. H.; Kochi, J. K. *J. Am. Chem. Soc.* **1975**, *97*, 1262. (b) Lemonovskii, D. A.; Fedin, V. P. *J. Organomet. Chem.* **1977**, *132*, C11. (c) Nesmeyanov, A. N.; Lemonovskii, D. A.; Fedin, V. P.; Perevalova, É. G. *Dokl. Akad. Nauk SSSR* **1979**, *245*, 609 (Eng. Translation **1979**, *245*, 142).

3. a) Cloke, F. G. N.; Day, J. P. *J. Chem. Soc., Chem. Commun.* **1985**, 967. b) Bandy, J. A.; Cloke, F. G. N.; Cooper, G.; Day, J. P.; Girling, R. B.; Graham, R. G.; Green, J. C.; Grinter, R.; Perutz, R. N. *J. Am. Chem. Soc.* **1988**, *110*, 5039.

4. Two lower row metallocene cations have been prepared: $(\eta^5\text{-}C_5Me_5)_2Os^+$ which can be isolated (O'Hare, D.; Green, J. C.; Chadwick, T. P.; Miller, J. S. *Organometallics* **1988**, *7*, 1335) and $(\eta^5\text{-}C_5Me_5)_2Ru^+$, which cannot be isolated, (Koelle, U.; Salzer, A. *J. Organomet. Chem.* **1983**, *243*, C27 and Kölle, U.; Grub, J. *J. Organomet. Chem.* **1985**, *289*, 133).

5. Hübel, W.; Merényi, R. *J. Organomet. Chem.* **1964**, *2*, 213.

6. Bruce, M. I.; Humphrey, P. A.; Williams, M. L.; Skelton, B. W.; White, A. H. *Aust. J. Chem.* **1989**, *42*, 1847.

7. Cotton, F. A.; Whipple, R. O.; Wilkinson, G. *J. Am. Chem. Soc.* **1953**, *75*, 3586.

8. Keller, H. J.; Wawersik, H. *J. Organomet. Chem.* **1967**, *8*, 185.

9. Fischer, E. O.; Wawersik, H. *J. Organomet. Chem.* **1966**, *5*, 559.

10. (a) El Murr, N.; Sheats, J. E.; Gieger, W. E.; Holloway, J. D. L. *Inorg. Chem.* **1979**, *18*, 1443. (b) Gusev, O. V.; Denisovich, L. I.; Peterleitner, M. G.; Rubezhov, A. Z.; Ustynyuk, N. A.; Maitlis, P. M. *J. Organomet. Chem.* **1993**, *452*, 219.

11. Zagorevskii, D. V.; Holmes, J. L. *Organometallics* **1992**, *11*, 3224.

12. Janiak, C.; Schumann, H. *Adv. Organomet. Chem.* **1991**, *33*, 291.

13. Castellani, M. P.; Geib, S. J.; Rheingold, A. L.; Trogler, W. C. *Organometallics* **1987**, *6*, 1703.

14. Schumann, H.; Janiak, C.; Khani, H. *J. Organomet. Chem.* **1987**, *330*, 347.

15. Hoobler, R. J.; Hutton, M. A.; Dillard, M. M.; Castellani, M. P.; Rheingold, A. L.; Rieger, A. L.; Rieger, P. H.; Richards, T. C.; Geiger, W. E. *Organometallics* **1993,** *12*, 116.

16. Grosser, D. K. *Cyclic Voltammetry*, VCH Publishers, New York, 1993.

17. (a) Dwyer, F. P.; Sargeson, A. M. *J. Am. Chem. Soc.* **1953**, *75*, 984. (b) Belyaev, A. V.; Venediktov, A. B.; Fedotov, M. A.; Khranenko, S. P. *Koord. Khim.* **1985**, *11*, 794.

18. Prolonged exposure of $(C_5HPh_4)_2Rh$ to the sodium amalgam produces a brown solid that is insoluble in THF.

19. Castellani, M. P.; Wright, J. M.; Geib, S. J.; Rheingold, A. L.; Trogler, W. C. *Organometallics* **1986**, *5*, 1116.

20. Hoobler, R. J.; Adams, J. V.; Hutton, M. A.; Francisco, T. W.; Haggerty, B. S.; Rheingold, A. L; Castellani, M. P. *J. Organomet. Chem.* **1991**, *412*, 157.

21. For all of the iron and cobalt group elements, the unsubstituted metallocene or metallocenium ion is formed under relatively mild conditions (generally a reflux below 80 °C for up to 24 h results in >70% yield). For the syntheses of $(C_5HPh_4)_2Fe$ and $(C_5HPh_4)_2Co$ comparable conditions to Cp_2M are employed with only small yield reductions.[13, 19] For both second-row compounds $(C_5HPh_4)_2Ru$ (160 °C, 48 h, 30% yield) and $(C_5HPh_4)_2Rh^+$ (160 °C, 5 d, 50% yield) the conditions are much harsher than for their respective C_5H_5 compound (Cp_2Ru: 80°C, 2 h, 70% yield, Cp_2Rh^+: 65 °C, 1 d, 70% yield). In each case, the third-row complexes, $(C_5HPh_4)_2Os$ and $(C_5HPh_4)_2Ir^+$, did not form even at 215 °C over several days. The third-row C_5H_5 analogues are prepared under similar conditions to their second-row counterparts, albeit with somewhat reduced yields. Since the second- and third-row metals are larger than those of the first-row, the differences in reactivity cannot arise from steric considerations. Rather the difference may arise from the fact that lower row metals frequently bind substrates more strongly than first-row metals.

In the case of the lower row metals, the $C_5HPh_4^-$ anion may have to displace a strongly

bound ligand. This would be difficult for a ligand as large and bulky as $C_5HPh_4^-$.

22. Pauling, L. *The Nature of the Chemical Bond*, 3rd Ed.; Cornell University Press: Ithaca, NY; p 256.

23. Bruce, M. I.; Rodgers, J. R.; Walton, J. K. *J. Chem. Soc., Chem. Commun.* **1981**, 1253.

24. Bard, A. J.; Faulkner, L. F. *Electrochemical Methods*, John Wiley and Sons, New York, 1980, pp 218-220.

25. Ref 24, pp 222-232.

26. Ref 24, pp 223.

27. Somewhat larger shifts with *v* were observed at Pt electrodes.

28. Ref 24, pp 225-227.

29. The dangers inherent to invoking structural changes to account slow heterogeneous charge transfer reactions have been noted by a number of researchers, including one of the authors: see Geiger, W.E. in Lippard, S.J. (ed) *Progress in Inorganic Chemistry*, John Wiley and Sons, New York, 1985, Vol 33.

30. Rieger, P.H. *Organometallic Radical Processes*, Trogler, W.C., Ed.; Elsevier: Amsterdam, 1990, pp 270-305.

31. (a) Dunbar, K. R.; Haefner, S. C. *Organometallics* **1992**, *11*, 1431. (b) Haefner, K. R.; Dunbar, K. R.; Bender, C. *J. Am. Chem. Soc.* **1991**, *113*. 9540.

32. (a) Ammeter, J. H. *J. Magn. Res*. **1978**, 299. (b) Rajasekharan, M. V.; Giezynski, S.; Ammeter, J. H.; Oswald, N.; Michaud, P.; Hamon, J. R.; Astruc, D. *J. Am. Chem. Soc.* **1982**, *104*, 2400. (c) Zoller, L.; Moser, E.; Ammeter, J. H. *J. Phys. Chem.* **1986***, 90*, 6632.

Table I. Crystal and Refinement Data for Octaphenylrhodocene.

a) Crystal Data

Formula	$C_{58}H_{42}Rh$
FW	841.8
Cryst System	Triclinic
Space Group	$P\bar{1}$
a, Å	8.622 (3)
b, Å	10.778 (4)
c, Å	12.894 (5)
α, deg	65.58 (3)
β, deg	72.66 (3)
γ, deg	83.52 (3)
V, Å^3	1041.4 (7)
Z	1
Color	Dark green
Crystal Size, mm	0.22 x 0.31 x 0.40
D (Calcd), g/cm^3	1.342
Abs Coeff, cm^{-1}	4.50

b) Data Collection

Diffractometer	Siemens P4
Radiation	graphite-monochromated Mo Kα ($\lambda = 0.710\ 73$ Å)
Temp, K	298
2θ Scan Range, deg	4.0 to 48.0
Scan Type	ω
Reflns Collcd	3137
Obsd Rflns	2479 ($F > 5.0\sigma(F)$)

c) Solution and Refinement

Solution   Direct Methods

Refinement Method   Full-Matrix Least-Squares

Quantity Minimized $\Sigma w(F_o - F_c)^2$

Weighting Scheme $w^{-1} = \sigma^2(F) + 0.0010F^2$

Number of Parameters Refined   281

Final R Indices (Obs. Data),% $R = 7.63$, $wR = 10.12$

R Indices (All Data), % $R = 15.77$, $wR = 13.62$

GOF   1.88

Data-to-Parameter Ratio   8.8:1

Largest Difference Peak, $e\text{Å}^{-3}$ 2.08

Largest Difference Hole, $e\text{Å}^{-3}$ -1.04

Table II. Atomic Coordinates (x10⁴) and Equivalent Isotropic Displacement Coefficients

(Å² x 10³) for Octaphenylrhodocene.

	x	y	z	U*
Rh	0	0	0	32 (1)
C(1)	2187 (9)	1193 (8)	-377 (7)	43 (4)
C(2)	2364 (9)	924 (9)	-1415 (7)	44 (4)
C(3)	2376 (9)	-551 (8)	-1021 (7)	41 (4)
C(4)	2312 (8)	-1138 (8)	230 (7)	39 (3)
C(5)	2304 (9)	-48 (8)	576 (7)	40 (4)
C(21)	1670 (10)	1777 (9)	-3357 (7)	47 (4)
C(22)	1663 (13)	2804 (11)	-4430 (9)	67 (5)
C(23)	2375 (16)	4042 (12)	-4788 (9)	86 (6)
C(24)	3111 (14)	4252 (11)	-4087 (9)	78 (6)
C(25)	3152 (11)	3213 (10)	-2986 (8)	57 (4)
C(26)	2411 (9)	1973 (9)	-2611 (7)	46 (4)
C(31)	1814 (11)	-2484 (10)	-1469 (9)	58 (5)
C(32)	2187 (16)	-3208 (12)	-2182 (13)	85 (7)
C(33)	3437 (21)	-2807 (17)	-3201 (14)	103 (10)
C(34)	4298 (16)	-1646 (15)	-3525 (9)	87 (7)
C(35)	3936 (11)	-914 (11)	-2828 (8)	64 (5)
C(36)	2672 (9)	-1312 (9)	-1795 (7)	45 (4)
C(41)	4147 (10)	-3096 (10)	586 (8)	55 (4)
C(42)	4479 (14)	-4453 (13)	1116 (11)	79 (6)
C(43)	3251 (15)	-5336 (12)	1940 (12)	84 (7)
C(44)	1701 (14)	-4878 (11)	2199 (11)	74 (6)
C(45)	1364 (11)	-3510 (9)	1652 (9)	57 (4)
C(46)	2588 (9)	-2601 (8)	836 (7)	42 (4)

C(51)	2752 (12)	-1324 (11)	2610 (9)	64 (5)
C(52)	2615 (13)	-1421 (12)	3731 (9)	73 (5)
C(53)	2004 (12)	-366 (12)	4053 (9)	68 (5)
C(54)	1585 (12)	793 (12)	3237 (9)	70 (6)
C(55)	1716 (10)	920 (10)	2105 (8)	52 (4)
C(56)	2259 (9)	-158 (9)	1775 (7)	45 (4)

[a]Equivalent isotropic U defined as one third of the trace of the orthogonalized $\mathbf{U}_{ij}$ tensor.

Table III. Selected Bond Distances (Å) and Angles (deg) for Octaphenylrhodocene.

Rh-CNT[a]	1.904	C(1)-Rh-C(2)	37.4 (4)
C(1)-C(2)	1.444 (14)	C(2)-Rh-C(3)	37.5 (3)
C(2)-C(3)	1.455 (12)	C(3)-Rh-C(4)	37.7 (3)
C(3)-C(4)	1.455 (12)	C(1)-Rh-C(5)	36.3 (3)
C(4)-C(5)	1.418 (14)	C(4)-Rh-C(5)	36.2 (4)
C(1)-C(5)	1.411 (10)	C(1)-C(2)-C(3)	106.4 (7)
Rh-C(1)	2.220 (9)	C(2)-C(3)-C(4)	107.5 (9)
Rh-C(2)	2.283 (7)	C(3)-C(4)-C(5)	107.6 (7)
Rh-C(3)	2.247 (7)	C(1)-C(5)-C(4)	108.9 (8)
Rh-C(4)	2.251 (7)	C(2)-C(1)-C(5)	108.9 (8)
Rh-C(5)	2.307 (9)	C(1)-C(2)-C(26)	125.3 (8)
		C(2)-C(3)-C(36)	126.0 (7)
		C(3)-C(4)-C(46)	120.5 (9)
		C(4)-C(5)-C(56)	126.8 (7)
		C(1)-C(5)-C(56)	124.0 (9)
		C(5)-C(4)-C(46)	130.5 (8)
		C(4)-C(3)-C(36)	125.8 (7)
		C(3)-C(2)-C(26)	128.2 (9)

[a]CNT = centroid of the cyclopentadienyl ring

Table IV. Phenyl Ring Torsion Angles (deg).

Cp Carbon	Angle
2	33.6
3	50.0
4	77.2
5	19.5

Table V. Formal Potentials of Some Rhodocenium Derivatives

Compound	Couple	Solvent	$E°$ vs Fc	Reference
$[(C_5HPh_4)_2Rh]^n$	n = +1/0	DMF	-1.44 V	this work
	n = 0/1-	DMF	-2.19 V‡	this work
$[(C_5H_5)_2Rh]^n$	n = +1/0	CH_3CN	-1.81 V	10a
	n = 0/1-	CH_3CN	-2.58 V	10a
$[(C_5Me_5)_2Rh]^n$	n = +1/0	THF	-2.38 V†	10b
	n = 0/1-*	THF	-3.34 V† (irrev)	10b
$[(C_5H_5)Rh(C_5Me_5)]^n$	n = +1/0	THF	-2.07 V†	10b
	n = 0/1-*	THF	-3.06 V (irrev)	10b
$[(C_5Me_5)Rh(C_9H_7)]^n$	n = +1/0	THF	-1.74 V	10b
	n = 0/1-*	THF	-2.44 V	10b

‡Value from CV simulation at Pt electrode.

*Potential vs Fc obtained by subtracting 0.56 V from quoted potential vs SCE.

†n = +1/0 is only partially chemically reversible, so assignment of second wave to 0/1- is in doubt.

Table VI. ESR Parameters for (C$_5$HPh$_4$)$_2$M.

M	T/K	g_x	g_y	g_z	tan α	kV
Rh	77	1.952	2.030	1.771	3.79(4)	0.452(5)
Rh	90	1.958	2.020	1.784	4.08(5)	0.458(5)
Rh	90	1.959	2.021	1.784	4.12(5)	0.462(6)
Rh	90	1.959	2.024	1.771	4.11(5)	0.488(6)
Rh	90	1.955	2.028	1.779	3.90(4)	0.445(5)
Co	77	1.999	2.095	1.884	5.84(14)	0.350(8)
Ni$^+$	77	2.018	2.072	1.884		

<u>Figure Cations</u>

Figure 1. Molecular structure and labeling scheme for $(\eta^5\text{-}C_5HPh_4)_2Rh$.

Figure 2. CV traces ($v = 0.2$ V/s) of reduction of $(\eta^5\text{-}C_5HPh_4)_2Rh^+$: (top, experimental) 0.4 mM solution of $[PF_6]$ salt in DMF at Pt electrode, T = ambient; (bottom, theoretical) $E_1^\circ =$ -1.44 V, $k_{s1} = 3$ cm/s, $\alpha_1 = 0.50$, $E_2^\circ = $ -2.13 V, $k_{s2} = 1.0 \times 10^{-3}$ cm/s, $\alpha_2 = 0.68$.

Figure 3. Voltammetry at rotating Pt electrode before (dotted line) and after (solid line) cathodic electrolysis of 0.5 mM solution of $[(\eta^5\text{-}C_5HPh_4)_2Rh][PF_6]$ in THF at $E_{appl} = $ -1.7 V, T = ambient.

Figure 4. Correlation of total reduction factor kV with increasing "orthorhombicity" tan α for d[7] metallocenes, after Ammeter.[32]
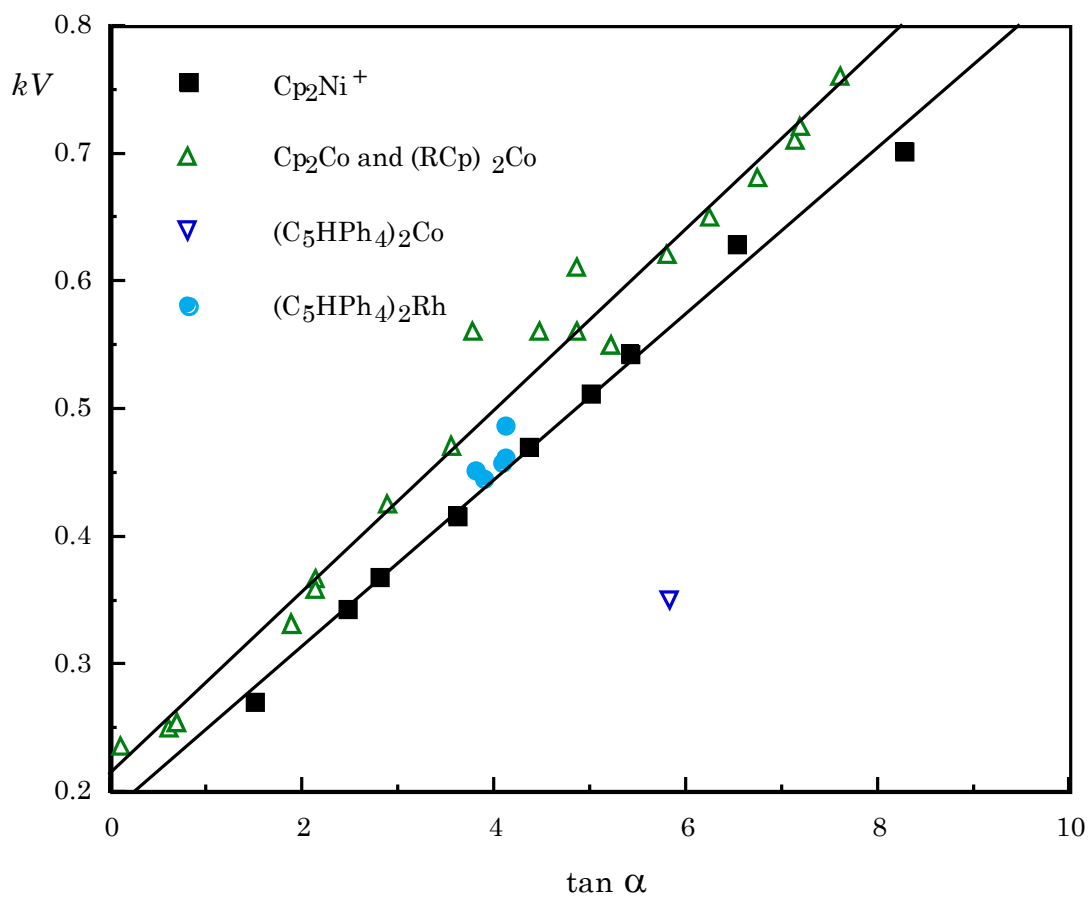
Supplementary Material

for

Synthesis, Characterization, and Molecular Structure of

Bis(tetraphenylcyclopentdienyl)rhodium(II)

by

J. E. Collins, M. P. Castellani, A. L. Rheingold, E. J. Miller,

W. E. Geiger, A. L. Rieger, and P. H. Rieger

Table 1S. Anisotropic Displacement Coefficients ($\text{Å}^2\text{x}10^3$).

	U_{11}	U_{22}	U_{33}	U_{12}	U_{13}	U_{23}
Rh	32 (11)	31 (1)	32 (1)	-3 (1)	-9 (1)	-11 (1)
C(1)	48 (5)	45 (5)	44 (5)	-4 (4)	-15 (4)	-23 (4)
C(2)	41 (4)	52 (5)	35 (4)	0 (4)	-6 (3)	-16 (4)
C(3)	35 (4)	39 (4)	46 (5)	-5 (3)	-4 (3)	-19 (4)
C(4)	34 (4)	45 (5)	35 (4)	2 (3)	-10 (3)	-12 (4)
C(5)	44 (4)	46 (5)	38 (4)	4 (4)	-16 (3)	-22 (4)
C(21)	55 (5)	50 (5)	34 (4)	-4 (4)	-8 (4)	-15 (4)
C(22)	88 (7)	67 (7)	46 (6)	-1 (5)	-22 (5)	-22 (6)
C(23)	139 (11)	58 (7)	39 (6)	-16 (7)	-12 (6)	-5 (6)
C(24)	111 (9)	49 (6)	56 (7)	-29 (6).	2 (6)	-14 (6)
C(25)	67 (6)	55 (6)	47 (5)	-7 (5)	-3 (4)	-25 (5)
C(26)	38 (4)	48 (5)	38 (4)	-3 (4)	0 (3)	-9 (4)
C(31)	66 (6)	55 (6)	72 (6)	10 (5)	-36 (5)	-35 (6)
C(32)	113 (9)	61 (7)	123 (11)	33 (7)	-78 (9)	-55 (8)
C(33)	160 (14)	113 (12)	99 (11)	76 (11)	-88 (11)	-85 (11)
C(34)	115 (9)	106 (10)	51 (6)	60 (8)	-33 (6)	-51 (8)
C(35)	67 (6)	75 (7)	51 (5)	25 (5)	-16 (5)	-33 (6)
C(36)	45 (4)	52 (5)	52 (5)	14 (4)	-23 (4)	-30 (5)
C(41)	51 (5)	59 (6)	56 (5)	16 (4)	-21 (4)	-25 (5)
C(42)	73 (7)	83 (8)	87 (8)	41 (7)	-40 (6)	-37 (8)
C(43)	98 (9)	54 (7)	103 (9)	33 (7)	-53 (8)	-27 (7)
C(44)	84 (7)	49 (6)	78 (8)	0 (5)	-26 (6)	-12 (6)
C(45)	60 (6)	46 (5)	57 (6)	11 (4)	-22 (4)	-14 (5)
C(46)	51 (5)	43 (5)	37 (4)	5 (4)	-19 (4)	-17 (4)
C(51)	84 (7)	66 (6)	57 (6)	11 (5)	-32 (5)	-33 (6)

C(52)	90 (7)	75 (7)	52 (6)	4 (6)	-35 (5)	-14 (6)
C(53)	76 (6)	95 (8)	45 (5)	5 (6)	-20 (5)	-39 (6)
C(54)	71 (6)	81 (8)	76 (7)	10 (5)	-20 (5)	-39 (6)
C(55)	47 (5)	68 (6)	45 (5)	6 (4)	-14 (4)	-27 (5)
C(56)	46 (4)	48 (5)	38 (4)	-7 (4)	-12 (3)	-13 (4)

[a]The anisotropic displacement factor exponent takes the form: $-2\pi^2(h^2a^{*2}U_{11} + ... + 2hka^*b^*U_{12})$

Table 2S. H-Atom Coordinates (x10⁴) and Isotropic Displacement Coefficients (Å²x10³).

	x	y	z	U
H(1)	2179	2080	-367	80
H(21)	ll60	914	-3106	80
H(22)	ll39	2656	-4931	80
H(23)	2360	4757	-5540	80
H(24)	3621	5115	-4339	80
H(25)	3677	3361	-2485	80
H(31)	940	-2782	-751	80
H(32)	1573	-4015	-1951	80
H(33)	3697	-3317	-3689	80
H(34)	5172	-1349	-4243	80
H(35)	4550	-107	-3059	80
H(41)	5007	-2470	17	80
H(42)	5567	-4776	925	80
H(43)	3479	-6285	2318	80
H(44)	841	-5503	2767	80
H(45)	276	-3187	1843	80
H(51)	3157	-2076	2393	80
H(52)	2931	-2243	4297	80
H(53)	1915	-437	4835	80
H(54)	1180	1545	3453	80
H(55)	1401	1743	1539	80